

Nickel-cobalt-titanate thin films – new sustainable magnetic oxides

Yukari Fujioka¹, Johannes Frantti¹, Christopher Rouleau², Alexander Puretzy², and Harry M. Meyer³.

¹ Finnish Research and Engineering, Jaalaranta 9 B 42, Helsinki 00180, Finland

² Center for Nanophase Materials Sciences, Oak Ridge National Laboratory, Oak Ridge, Tennessee, 37831, USA

³ Oak Ridge National Laboratory, Oak Ridge, Tennessee, 37831, USA

Abstract

An extension of nickel-cobalt-titanate ($\text{Ni}_{1-x}\text{Co}_x$) TiO_3 (NCT), $A_{1+2x}\text{Ti}_{1-x}\text{O}_3$, where A is Ni^{2+} , Co^{2+} and $-0.25 < x < 1$, is demonstrated by thin films grown by pulsed laser deposition. In Ti-poor region a thin film crystal structure not stable in bulk form was prepared. The structure is obtained by filling octahedra vacant in the corundum and ilmenite structures. When $x = 1$ all vacant sites are filled. Nickel-cobalt-titanate materials can be deposited as high-quality thin films on cheap substrates. A direct overlap between the adjacent cation d -orbitals result in a bond formation and magnetic interactions between the cations. This serves as a route to tailor functional properties. NCT-based materials are non-toxic and cheap, stable in the air, have tunable composition, and are producible in a sustainable manner. Here we report the structural properties of thin films as a function of Ti/(Ni+Co) ratio.

1. Introduction

One route to look for alternative materials is to systematically modify the composition of the prevailing materials. Correspondingly, the number of work dedicated to perovskites is immense. Another, less studied alternative materials are ilmenite oxides [1-7], which are structurally similar to the lithium niobate [8] and the corundum structures [2]. There are two structural features which makes the ilmenite and corundum structures particularly appealing, presence of short cation-cation distances and vacant octahedra sites. Nickel-cobalt-titanate ($\text{Ni}_{1-x}\text{Co}_x$) TiO_3 (NCT) ilmenite solid-solution exhibits triclinic structure and spontaneous magnetization and so possesses a potential for electronic applications requiring ferromagnetic properties. The shortest cation-cation distances in NCT are 2 Å, to be compared to 3.9 Å found in the perovskite lead titanate. Vacant sites open up new tailoring possibilities (examples are given in ref. 9), which is exploited in the present study. Thin film properties often deviate from the corresponding bulk properties. Especially the layer composition can be controlled which makes it possible to achieve structures not stable in a bulk form. Lattice mismatch between the film and substrate causes strain being a one route to develop ferroelectric and ferromagnetic NCT thin films. In this paper we report the structural properties of NCT and NCT-derived thin films.

Common reasons to develop sustainable materials are to replace toxic materials, find economical alternatives or to find technologically better materials. The restriction of the use of Hazardous Substances (RoHs) requires heavy metals such as lead, mercury, cadmium, and hexavalent chromium to be substituted by safer alternatives [10]. Heavy metals are raw material for many high performance functional compounds applied in electronics. Rare earth elements (REE) are widely used in strong permanent magnets. Triggered by the REE price peak in 2011 efforts were launched to find sustainable and cheaper alternative materials

[11]. Surface oxidation is a serious technological problem in many REE magnets and evidently even more critical issue for thin films [12]. Though REE magnets have excellent magnetic properties, there are numerous applications which do not require extreme magnetization values. This opens up routes to develop new sustainable materials solving the other issues as shown below.

2. Why ilmenites – structural aspects

Ilmenite ABO_3 oxides possess unique structural features enabling rich functionality. The structure, Fig. 1, is layered; AO_6 and BO_6 octahedra alternate along the hexagonal c axis [13]. Each layer consists of two slightly separated, two-dimensional triangular cation nets. The separation is due to the electrostatic repulsion which is minimized by displacing the cations towards vacant octahedra, see Fig. 1 (a). As is discussed below, the vacant octahedra have a crucial role for stabilizing a new structure. The octahedra share edges in the layers, see Fig. 1 (b), between the layers the octahedra are connected by sharing faces, Fig. 1 (a). Besides oxygen and two-oxygen mediated magnetic interactions [14] the direct overlap between the adjacent d -orbitals in ilmenites results in a bond formation and additional magnetic interactions between the cations. This is in contrast to the perovskite structure in which octahedra share only corners. The short cation-cation distances are actually a factor behind the Pauling's third rule according to which the existence of edges and particularly of faces, common to two anion polyhedra in a coordinated structure decreases its stability [15]. This implies that the structures possessing these properties are generally not energetically favorable.

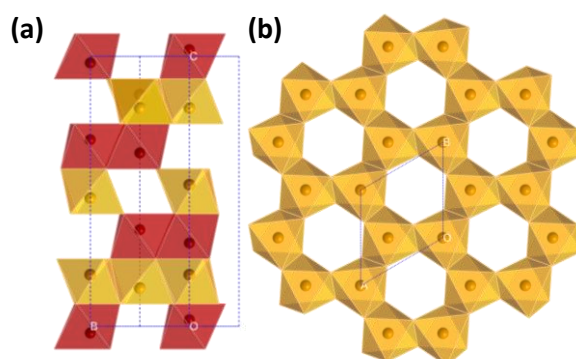


Fig. 1. The ilmenite structure. Red and gold-colored octahedra are Ti- and Ni/Co octahedra, respectively. Panel (a) gives an bc -plane projection and panel (b) shows an ab -plane projection. For clarity, only Ni/Co-octahedron network is shown in panel (b). The structure is consisted of octahedra of which 1/3 are vacant.

Neutron and synchrotron x-ray diffraction [6] and Raman scattering [16] studies revealed that NCT in a bulk form possesses a lower crystal symmetry than $R\bar{3}$ and also two magnetic phases absent in $NiTiO_3$ and $CoTiO_3$. $NiTiO_3$ [17] and $CoTiO_3$ [18] are reported to have $R\bar{3}$ symmetry. $x = 0.50$ NCT is ferromagnetic below 70 K [6,7]. Both crystal distortion and magnetism were assigned to the interactions between cations, there being interactions through octahedral edges via t_{2g} orbital overlap between $Ni^{2+}-Ni^{2+}$, $Co^{2+}-Co^{2+}$, and $Ni^{2+}-Co^{2+}$ cation pairs within the ab -plane. There is also an orbital overlap interaction between the layers. Each Ni/Co-layer octahedra share a face with Ti-layer octahedra only on one side of the layer, see Fig. 1(a). An implication of this is that the half-filled t_{2g} Co orbital can ferromagnetically couple with an empty Ti t_{2g} orbital if there is a partially occupied state at Ti (e.g., some Ti-cations are in a Ti^{3+} state) which is orthogonal to the empty Ti state [19]. Interestingly, a reversible structural transformation from ilmenite structure with alternating Ti-Ni/Co layers to the corundum structure with mixed Ti/Ni/Co layers took place during heating in $x = 0.50$ sample, indicating that the interactions between Ni/Co and Ti cations are strongly temperature

dependent [16]. Thus, by adjusting the Ni-Co-Ti distribution one can control the magnetic properties and crystal distortion or even structure. For this purpose pulsed laser deposition (PLD) is an excellent method. We note that similar features to the NCT are also seen in iron oxides, including a solid solution of α -Fe₂O₃ and FeTiO₃ [20].

3. Experimental

NCT thin films were deposited by PLD technique at the Center for Nanomaterials Sciences (CNMS) on sapphire substrates with 0001 (MTI Corporation) and 11 $\bar{2}$ 0 and 10 $\bar{1}$ 0 (Mateck) planes. Three targets, NiTiO₃, CoTiO₃ and NiCoO₄ were ablated repeatedly. Shot ratios and total number of shots were adjusted to control the composition and film thickness and the targets were rotated during ablation. Substrates were in-situ heated. Laser beam wavelength was 248 nm and the pulse repetition rate was 10 Hz. Table 1 summarizes the deposition conditions and thin film composition as detected by X-ray photoelectron spectroscopy (XPS).

Table 1. Summary of the deposition conditions and composition as determined by XPS. *T* is substrate temperature, *p*O₂ is O₂ pressure and Fluence is the laser beam pulse energy per area. The composition of the sample H was estimated from the known compositions of three thin films deposited under similar conditions.

Sample	Composition	<i>p</i> O ₂ (mTorr)	<i>T</i> (°C)	Fluence (Jcm ⁻²)	Substrate
A	Ni _{0.32} Co _{0.24} Ti _{1.35} O ₃	5	475	4.8	Al ₂ O ₃ (11 $\bar{2}$ 0)
B	Ni _{0.46} Co _{0.18} Ti _{1.35} O ₃	5	475	3.0	Al ₂ O ₃ (11 $\bar{2}$ 0)
C	Ni _{0.46} Co _{0.81} Ti _{0.82} O ₃	10	590	3.0	Al ₂ O ₃ (0001)
D	Ni _{0.49} Co _{0.92} Ti _{0.70} O ₃	10	500	3.0	Al ₂ O ₃ (0001)
E	Ni _{1.07} Co _{1.72} O ₃	10	610	3.0	Al ₂ O ₃ (0001)
F	Ni _{1.07} Co _{1.72} O ₃	10	610	3.0	Al ₂ O ₃ (10 $\bar{1}$ 0)
G	Ni _{1.07} Co _{1.72} O ₃	10	610	3.0	Al ₂ O ₃ (11 $\bar{2}$ 0)
H	Ni _{0.78} Co _{1.02} Ti _{0.46} O ₃	10	610	3.0	Al ₂ O ₃ (0001)
I	Ni _{0.78} Co _{1.02} Ti _{0.46} O ₃	10	610	3.0	Al ₂ O ₃ (10 $\bar{1}$ 0)
J	Ni _{0.57} Co _{0.69} Ti _{1.17} O ₃	10	610	3.0	Al ₂ O ₃ (0001)

Raman measurements were performed using a Jobin-Yvon T64000 spectrometer consisting of a double monochromator coupled to a third monochromator stage with 1800 grooves per millimeter grating (double subtractive mode). A liquid nitrogen cooled charge-coupled device detector was used to count photons. All measurements were carried out under a microscope in backscattering configuration. Raman spectra were excited using a continuous wave solid-state laser (wavelength 532 nm).

X-Ray Diffraction (XRD) data on thin films were collected by Panalytical X'Pert Pro MPD diffractometer with a CuK α source, Ni filter and X'Celerator detector.

XPS measurements were conducted for the determination of the film composition as a function of depth (XPS, K-Alpha XPS system, Thermo Fisher Scientific) equipped with a monochromated Al-K α source ($h\nu = 1486.6$ eV) and argon ion sputtering.

4. Results

Figure 2 shows XRD patterns measured from NCT thin films. Except for sample B, only (00 l) type peaks were detected, indicating a preferred orientation of the films grown on (0001) sapphire. In the case of prototype ilmenite structure this would imply that the hexagonal *c*-axis is perpendicular to the substrate plane. Since

strain and non-prototype composition can lower the symmetry this may no longer be true. Samples A and B were grown on (11 $\bar{2}$ 0) sapphire substrates, the most apparent difference being the larger laser pulse energy applied in the growth of film A which could be the reason why, somewhat surprisingly, the film had preferred 00/ orientation. Below we give further results for other films grown with similar pulse energies as samples B, C and D, which also indicate that films grown with modest pulse energies on (0001) sapphire substrates have preferred 00/ orientation. It is also shown that except of the sample B, films grown on (11 $\bar{2}$ 0) sapphire substrates were either 00/ oriented.

Though the peak positions match with the ilmenite structure the intensity ratios of the peaks do not correspond to a case in which (Ni,Co) and Ti are segregated in their own layers (Model 1), as is shown by Table 2. Since the data for samples A, C and D allow only a determination of the *c*-axis length, we assumed that the space group symmetry is $R\bar{3}$ and constrained the *a* axis length of NiTiO₃, 5.031 Å [6]. Also the fractional coordinates of ions were constrained. Two simple models were tested, Model 1 assumes that (Ni²⁺,Co²⁺) and Ti⁴⁺ ions prefer own layers as in the ideal ilmenite structure. Model 2 assumes that all layers are compositionally equivalent and contain cations in the composition ratios given in Table 1. Models 1 and 2 are given in Table 3 in Appendix 1. Occupancies for samples A, C and D are given in Table 3. The *c* axis was 13.8114, 14.5800 and 14.5846 Å for samples A, C and D, respectively.

Table 2 gives intensity ratios when all cations are assumed to be mixed in the same layer in the composition ratios (Model 2) given in Table 1.

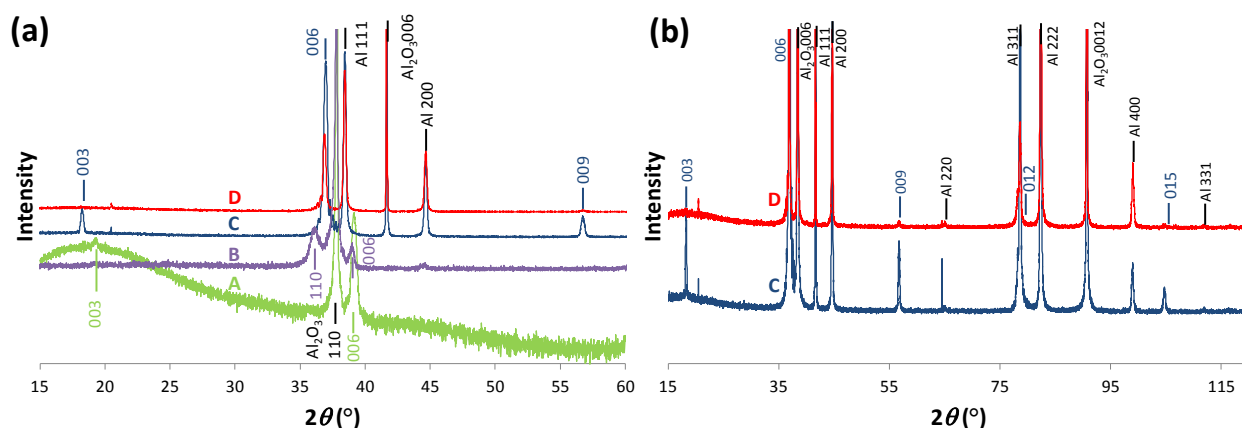


Fig. 2. (a) XRD patterns measured from thin films A, B, C and D. The reflections from all films were indexed by a single ilmenite structure. Also reflections from the sapphire substrates and the aluminum sample stage are given. To confirm the single phase nature and to observe (0012) and (0015) reflections a larger scan was carried out for the samples C and D.

Table 2. Measured and modeled intensity ratios of the 00/ reflections for samples A, C and D.

<i>l</i>	Sample A			Sample C			Sample D		
	Measured	Model 1	Model 2	Measured	Model 1	Model 2	Measured	Model 1	Model 2
3	0.12(3)	1	0	0.03(1)	1	0	0.017(2)	0.999	0
6	1	0.439	1	1	0.624	1	1	1	1
9	-	0.000	0	0.03(1)	0.000	0	0.021(1)	0	0
12	-	0.013	0.040	0.26(6)	0.000	0.012	0.41(2)	0.000	0.011
15	-	0.001	0	0.013(3)	0.001	0	0.02(2)	0.001	0

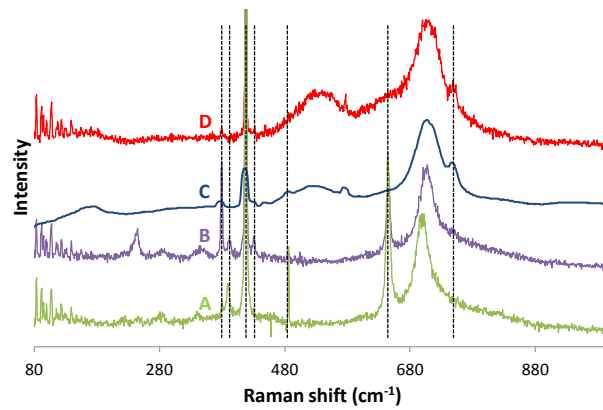


Fig. 3. Raman spectra measured from films A, B, C and D. Spectra measured from samples A and B are reminiscent to the ilmenite structure, whereas spectrum measured from sample D lacks the weak details between 200 and 400 cm^{-1} . Dotted lines indicate sapphire lines from substrate.

Though the non-zero intensities of the $003n$, n odd, peaks show that Model 2 cannot be correct, it gives some features correctly in the case of sample D: the intensities of the 006 and 0012 reflections are strong, whereas the 003, 009 and 0015 reflections are all weak even though not exactly zero. The tendency of 003 peak to get weaker with increasing $(\text{Ni}+\text{Co})/\text{Ti}$ ration is seen. Though Model 1 explains the presence of the 003 peak, it should be modified since the predicted 003 intensity is larger than observed. Some level of segregation of Ti and (Ni,Co) cations occurs, though all types of cations are found in the same layer. It is also probable that vacant octahedral sites gradually become occupied with increasing (Ni,Co) concentration, as is discussed below.

Raman scattering measurements is in line with the XRD results. Fig. 3 shows that the samples possessing large 003 peak also have several peaks between 200 and 400 cm^{-1} , in addition to the strong peak observed at around 700 cm^{-1} . The spectra collected from samples A and B are similar to the spectra collected on bulk NCT samples [16] and are characteristic to the ilmenite structure. Spectrum measured from sample D is significantly simpler and is characterized by a strong band between 450 and 800 cm^{-1} . Raman scattering results are consistent with the XRD results shown in Fig. 2 and are interpreted in terms of a structural transformation.

XPS measurements as a function of film thickness indicated that the film composition was essentially constant, as shown in Fig. 4. The valence state of Ni, Co and Ti cations were found to be 2+, 2+ and 4+, respectively. Despite there being a large charge difference between the cations present in the same layer, no evidence for the lithium niobate or other charge-ordered structure was found. Large charge difference is often accompanied by cation ordering. Nearly random distribution of cations is probably related to relative low *in-situ* substrate temperatures, see Table 1. Higher substrate temperatures would increase cation diffusion during film growth.

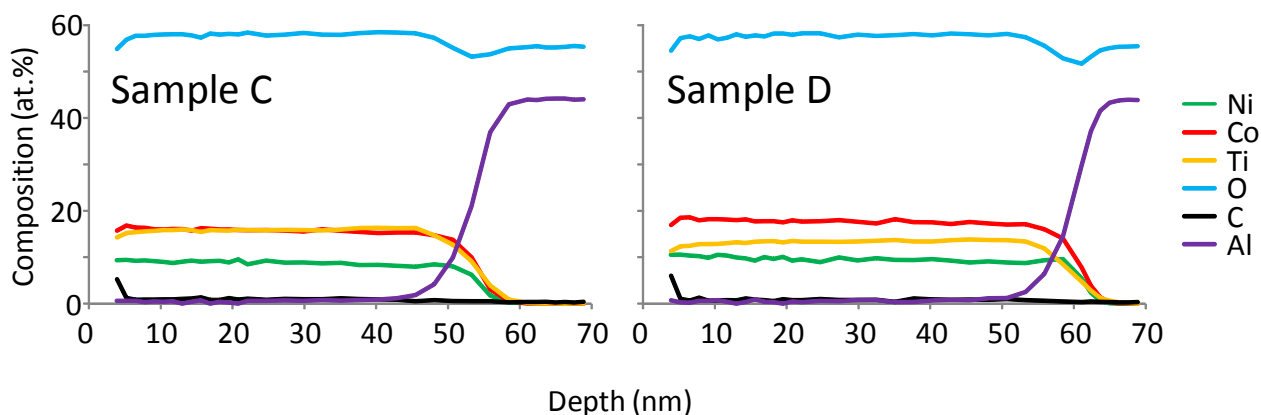


Fig. 4. The composition of the films C and D as a function of thickness. The composition is seen to be homogeneous throughout the film thickness. Substrate is marked by an increase in Al-signal.

To gain better understanding of the structural changes a set of Ti-deficient thin film were grown. Fig. 5 shows XRD patterns and Raman spectra measured from sample E, F, G, H, I and J with compositions tabulated in Table 1, the difference between samples H and I being different film orientation due to the different substrate orientation. Again, only 00/ reflections are observed from films deposited on 0001-oriented sapphire substrates, whereas 104 and 214 reflections are observed from film I deposited on a $10\bar{1}0$ -oriented sapphire substrate. The 104 reflection is rather weak, in contrast to a simulated $(\text{Ni}_{0.38}\text{Co}_{0.62})\text{O}_3$ intensities of the corundum structure in which the 104 reflection is the strongest and 214 has about one third of its intensity. The crystal structure of the film I is also the same as the structure of the 00/-oriented films. The XRD pattern Fig. 5(a), and Raman spectra, Fig. 5(d), of the sample J is rather typical for the ilmenite structure, whereas there are continuous changes with decreasing Ti-content, as Figs. 5(a) and (b) show. The Raman peak at around 700 cm^{-1} and the band at around 170 cm^{-1} (both spectral areas shadowed) become weaker with decreasing Ti-content and eventually these features are lacking from the spectrum collected on the sample E possessing no Ti. The XRD pattern of the sample E exhibits only 006 and 0012 reflections. Interestingly, also sample G is 00/ oriented, whereas sample F exhibits only 214 reflection and 104 reflection is absent. Thus, the structure of the samples E, F and G is not the simple corundum but is a derivative structure.

XPS measurements showed that the valences were +2 for Ni and Co cations and +4 four Ti cations. This would violate the charge neutrality condition if only 2/3 of the octahedra were occupied. An evident way to preserve charge neutrality is to place “excess” Co^{2+} and Ni^{2+} cations into the vacant octahedra. Thus, every Ti^{4+} cation replaced by a $\text{Ni}^{2+}/\text{Co}^{2+}$ -cation results in an occupation of a vacant octahedron. This corresponds to a decrease in oxygen/cation ratio following a formula $\text{A}^{2+}_{1+2x}\text{Ti}^{4+}_{1-x}\text{O}_3$, where A^{2+} is $\text{Ni}^{2+}/\text{Co}^{2+}$ -cation. x can also be negative, meaning that each “excess” Ti-cation is compensated for by a forming vacant octahedron. To gain further understanding the film compositions, including oxygen content, were determined through XPS measurements. As Fig. 6 shows, the measured $\text{O}/(\text{Ni}+\text{Co}+\text{Ti})$ ratios are close to the values expected for the vacancy filling model, especially in the Ti-poor region. In the Ti-rich area some deviation occurs, probably due to the formation of Ti^{3+} . Ti_2O_3 has the corundum crystal structure in which all Ti-cations are in the Ti^{3+} valence state. Based on the proposed vacancy filling model the sample E has a structure in which all sites vacant in the ilmenite/corundum structures are filled.

Our preliminary squid measurements indicate that the films possess very clear remnant magnetization. Next stage is to address in detail the magnetic and ferroelectric properties of the films.

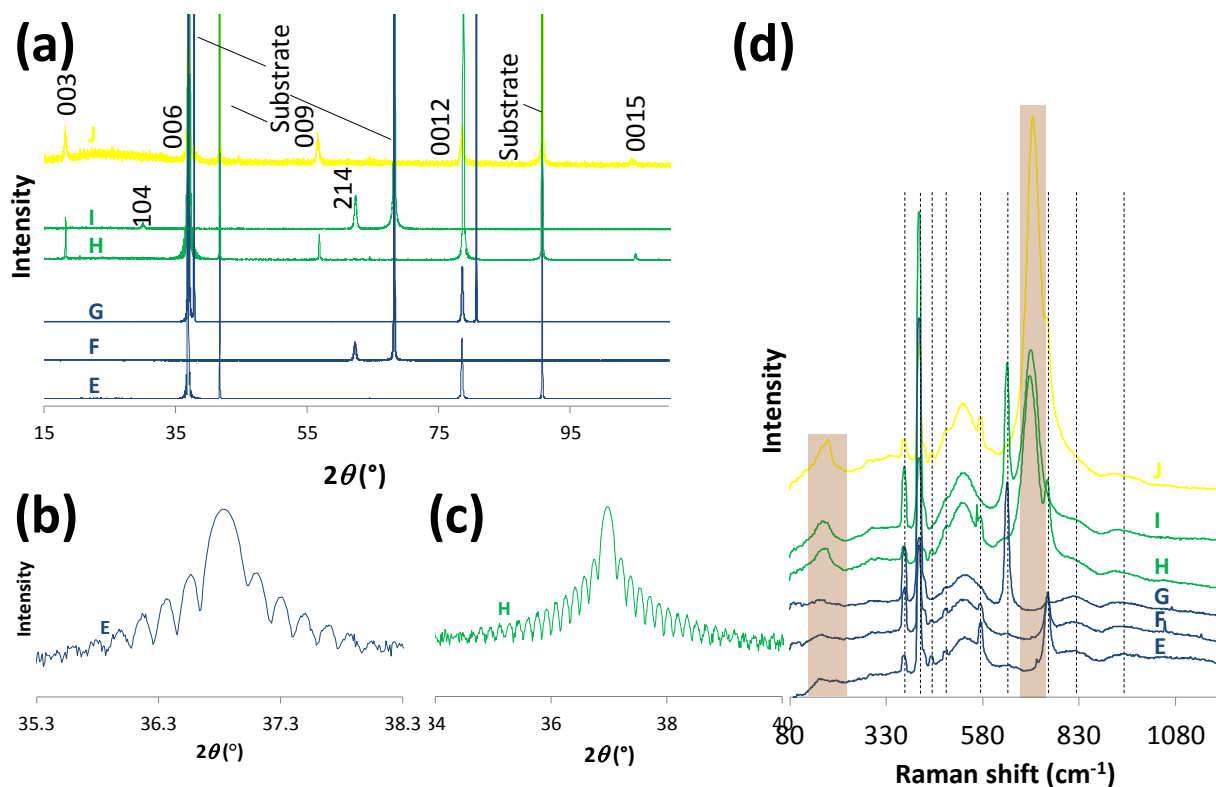


Fig. 5. (a) XRD pattern measured from samples E, F, G and H. Panels (b) and (c) show the XRD intensity of the 006 reflection of the E and F samples, respectively. Subsidiary minima are clearly revealed, consistently with the idea that the reflections originate from a single phase. Panel (d) gives the corresponding Raman spectra.

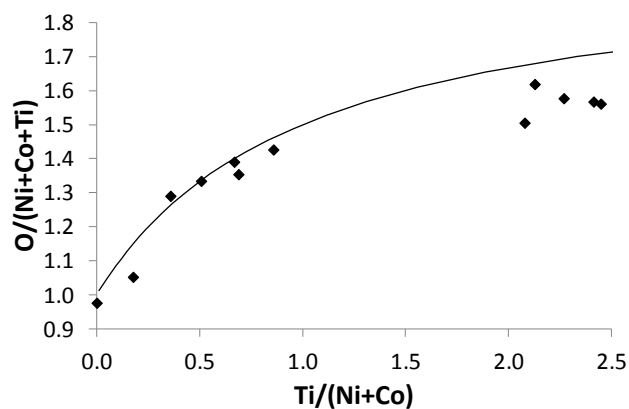


Fig. 6. Measured oxygen per cation ratios as a function of Ti/(Ni+Co) ratio. The line shows the $O/(Ni+Co+Ti)$ ratio as a function of Ti/(Ni+Co) ratio for $A_{1+2x}Ti_{1-x}O_3$.

Conclusions

Structural characteristics, especially the role of 3d orbital overlapping, of nickel-cobalt-titanate (NCT) behind the functional properties were summarized. Single phase thin films were deposited by pulsed laser deposition. Thin films contrasted bulk materials in two essential ways. First, films in which Ni, Co and Ti cations are mixed in the same layers were formed at relatively low temperatures. Second, both Ti-rich and

Ni/Co-rich films were formed with a new structure. A structural model in which vacant octahedra of the corundum structure are filled was constructed. One can continuously fill the vacant octahedra sites and transform from the ilmenite to the structure which is the corundum structure with no vacant octahedra. Further efforts are dedicated to address the properties of NCT for multiferroic applications.

Acknowledgments

All experimental work was conducted at the Center for Nanophase Materials Sciences, which is a DOE Office of Science User Facility. We thank Dr. Jong Keum (Oak Ridge National Laboratory) for his help with XRD and XRR measurements. None of the authors have any competing interests in the manuscript.

References

- [1] Goodenough J B. J. Appl. Phys. 1960; 31: S359-S361.
- [2] Rohrer G S. Structure and Bonding in Crystalline Materials. Cambridge: Cambridge University Press; 2001.
- [3] Posnak E, Barth T F W. Z. Kristallogr. 1934; 88: 271-274.
- [4] Fujioka Y, Frantti J, Nieminen R M. Phys. Chem. C. 2011; 115: 1457-1463.
- [5] Fujioka Y, Frantti J, Nieminen R M. Mater. Sci. Forum. 2012; 700: 23-27.
- [6] Fujioka Y, Frantti J, Llobet A, King G, Ehrlich S. Materials Today: Proceedings. 2016; 3: 265-276.
- [7] Fujioka Y, Frantti J. Arxiv 1111.6140v1.
- [8] Lines M E, Glass A M. Principles and Applications of Ferroelectrics and Related Materials. Oxford: Clarendon Press; 2001.
- [9] Fujioka Y, Frantti J, *et al.* Phys. Chem. C. 2012; 116: 17029–17039.
- [10] Directive 2002/95/EC of the European Parliament and of the Council of 27 January 2003 on the restriction of the use of certain hazardous substances in electrical and electronic equipment.
- [11] Rare Earth Alternatives in Critical Technologies (REACT) funding program. ARPA-E. <http://arpa-e.energy.gov/?q=arpa-e-programs/react>.
- [12] Campbell P. Permanent Magnet Materials and their Application. Cambridge: Cambridge University Press; 1994.
- [13] The hexagonal lattice is often only approximately correct due to crystal distortions.
- [14] Goodenough J B, Stickler J J. Phys. Rev. 1967; 164: 768-778.
- [15] Pauling L. J. Amer. Chem. Soc. 1929; 51: 1010-1026.

- [16] Fujioka Y, Frantti J, *et al.* Raman study of the structural distortion in $\text{Ni}_{1-x}\text{Co}_x\text{TiO}_3$ solid-solution. To be published.
- [17] Shirane G, Pickart S J, Ishikawa Y. J. Phys. Soc. Jpn. 1959; 14: 1352-1360.
- [18] Newnham R E, Santoro R P, Fang J H, Acta Cryst. 1964; 17: 240-242.
- [19] Goodenough J B. Magnetism and the Chemical Bond. New York: John Wiley & Sons, Inc.; 1963.
- [20] Chikazumi S. Physics of Ferromagnetism. Oxford: Oxford University Press; 2009.

Appendix 1

Table 3. Structural parameters for Models 1 and 2. Space group for both models is $R\bar{3}$. Axis setting is hexagonal. For Model 2, 003, 009, 0015, 003*n*, *n* is odd reflections vanish by symmetry.

Atom	x	y	z	Model 1			Model 2		
				Occupancy			Occupancy		
				A	C	D	A	C	D
Ni1	0	0	0.642	0.352	0.362	0.348	0.168	0.220	0.232
Co1	0	0	0.642	0.264	0.638	0.652	0.126	0.388	0.436
Ti1	0	0	0.642	0.385	0	0	0.707	0.392	0.332
Ni2	0	0	0.858	0	0.090	0.128	0.168	0.220	0.232
Co2	0	0	0.858	0	0.158	0.241	0.126	0.388	0.436
Ti2	0	0	0.858	1	0.752	0.631	0.707	0.392	0.332
O	0.305	0.015	0.250	1	1	1	1	1	1